Electronic Supplementary Information for:

Chemical looping of metal nitride catalysts: Low-pressure ammonia synthesis for energy storage

R. Michalsky,[*abc] A. M. Avram,[a,‡] B. A. Peterson,[a,#] P. H. Pfromm[a] and A. A. Peterson[b]

[a] Department of Chemical Engineering, 1005 Durland Hall, Kansas State University, Manhattan, Kansas 66506, United States, [b] School of Engineering, 184 Hope Street, Brown University, Providence, Rhode Island 02912, United States. [c] ETH Zürich, Department of Mechanical and Process Engineering, Sonneggstrasse 3, 8092 Zürich, Switzerland

Corresponding Author

[*] E-mail: michalskyr@ethz.ch. Telephone: +41 44-6338383.

Overview

1. Computational details

1.1 Local optimization procedures

The adsorption energies of H^* and OH^* at the stoichiometric $Mn_2N(0001)$ and $Sr_2N(001)$ surfaces were computed by placing an adsorbate at a unique, non-symmetric, initial adsorption position, *i.e.*, on-top a metal atom, at bridge sites between two metal atoms, at three-fold metal sites with a lower vacant interstitial (TFM) or lower lattice nitrogen, and minimizing the total electronic energy of the system to extract the optimized adsorption geometry. For both metal nitride surfaces the TFM site was determined as the preferred adsorption site for H^* and OH^* adsorbates. Thus, the adsorption of various ML NH_x^* (x = 0, 1, 2 or 3), H^* and OH^* was computed with the nitrogen species adsorbed above the source of the nitrogen, *i.e.*, above a nitrogen vacancy, and H^* and OH^* adsorbed at the TFM sites at maximum distance to the surrounding co-adsorbates.

1.2 Reference energies

The reported adsorption and reaction energies are relative to stable gas phase molecules, *i.e.*, the energy of the adsorbate A in the gas phase, E_A^{r}, is either the total electronic energy, E, of a stable gas phase molecule, *i.e.*, NH_3, H_2O and H_2, or derived from the energy of these molecules:

(S1) $E_{\mathrm{H}}^{\mathrm{r}} \equiv E[\mathrm{H_2}]/2$

(S2) $E_{\mathrm{N}}^{\mathrm{r}} \equiv E_{\mathrm{N_L}}^{\mathrm{r}} = E[\mathrm{NH_3}] - 3/2 \times E[\mathrm{H_2}]$

(S3) $E_{\mathrm{NH}}^{\mathrm{r}} \equiv E[\mathrm{NH_3}] - E[\mathrm{H_2}]$

(S4) $E_{\mathrm{NH_2}}^{\mathrm{r}} \equiv E[\mathrm{NH_3}] - E[\mathrm{H_2}]/2$

(S5) $E_{\mathrm{O}}^{\mathrm{r}} \equiv E[\mathrm{H_2O}] - E[\mathrm{H_2}]$

(S6) $E_{\mathrm{OH}}^{\mathrm{r}} \equiv E[\mathrm{H_2O}] - E[\mathrm{H_2}]/2$

where $E_{\mathrm{N}}^{\mathrm{r}}$ and $E_{\mathrm{NL}}^{\mathrm{r}}$ are the identical reference energy for atomic nitrogen either adsorbed at the surface or as part of the crystal lattice.

1.3 Free energy corrections

Gibbs free energies at T = 298.15 K and 1.013 bar total pressure, G_i, are calculated as below:

(S7) $G_i = H_i - \mathrm{T}S_i = E_i + U_{ZPE,i} - \mathrm{T}S_i$

where H_i and S_i are the enthalpy and entropy of an atomic geometry i respectively, E_i is the DFT-calculated electronic energy and $U_{\mathrm{ZPE},i}$ is the zero-point vibrational energy (S_i and $U_{\mathrm{ZPE},i}$ are taken into account for molecular species while they are neglected for the surface models; the free energy of nitrogen adsorbates and nitrogen vacancies are treated equally, see Eq. S2). All thermodynamic properties were calculated with vibrational frequencies and standard statistical mechanical equations evaluated through the Atomic Simulation Environment.[1]

1.4 Surface energetics

To characterize the surface reactivity, four additional quantities are provided with Table S2:

$\Delta G_{vac}[N^*, OH^*, H^*]$, *i.e.*, the net-energy that is required to form ¼ MLv_N and ¼ ML N^*, and ¼ ML OH^* and ¼ ML H^* from H_2O in the gas phase:

$$\text{(S8)}\quad \Delta G_{vac}[N^*, OH^*, H^*] \equiv G_s[N^*, OH^*, H^*] - (G_s + G^r_{H2O})$$

where $G_s[N^*, OH^*, H^*]$, G_s and $G_{H2O}{}^r$ are the total electronic energies of the surface with ¼ MLv_N, ¼ ML N^*, ¼ ML OH^* and ¼ ML H^*, the stoichiometric surface and of H_2O in the gas phase.

$\Delta G_{hyd}[NH^*, OH^*]$, *i.e.*, the energy required to hydrogenate ¼ ML N^* in the presence of ¼ ML OH^* with ¼ ML co-adsorbed H^*:

$$\text{(S9)}\quad \Delta G_{hyd}[NH^*, OH^*] \equiv G_s[NH^*, OH^*] - G_s[N^*, OH^*, H^*]$$

where $G_s[NH^*, OH^*]$ is the energy of the surface with ¼ MLv_N, ¼ ML NH^* and ¼ ML OH^* and $G_{hyd}[N^*, OH^*, H^*]$ is the energy of the surface with ¼ MLv_N, ¼ ML N^*, ¼ ML OH^* and ¼ ML H^*.

$\Delta G_{oxi}[N^*, 2H^*]$, *i.e.*, the net-energy required to form ¼ MLv_N that is filled with lattice oxygen, O_L, derived from the cleavage of H_2O yielding a partly oxidized surface covered with ¼ ML N^* and ½ ML H^*:

$$\text{(S10)}\quad \Delta G_{oxi}[N^*, 2H^*] \equiv G_s[O_L, N^*, 2H^*] - (G_s + G^r_{H2O})$$

where $G_s[O_L, N^*, 2H^*]$ is the energy of the surface with ¼ MLv_N that is filled with O_L and covered with ¼ ML N^* and ½ ML H^*.

$\Delta G_{oxi,hyd}[NH^*, H^*]$, *i.e.*, the energy required to hydrogenate ¼ ML N^* on an oxynitride surface with ¼ ML O_L with ½ ML co-adsorbed H^*:

$$\text{(S11)}\quad \Delta G_{oxi,hyd}[NH^*, H^*] \equiv G_s[O_L, NH^*, H^*] - G_s[O_L, N^*, 2H^*]$$

where $G_s[O_L, NH^*, H^*]$ is the energy of the surface with ¼ MLv_N that is filled with O_L and covered with ¼ ML NH^* and ¼ ML H^*.

2. Experimental details

2.1 Metal nitride characterization

Table S1: Characterization of binary metal nitrides

phase [A]	ε-Mn_4N (ζ-$Mn_6N_{2.58}$)	α-Ca_3N_2 (Ca_2N)	Sr_2N
space group [A]	$Pm\bar{3}m$ ($P6_322$)	$Ia\bar{3}$ ($R\bar{3}m$)	$R\bar{3}m$
d_p (μm) [B]	46 ± 19	105 ± 25	125 ± 46
A_{BET} ($m^2\ kg^{-1}$) [C]	270 ± 3	1253 ± 6	1048 ± 4
Φ (vol.%) [D]	62 ± 1	55 ± 3	53 ± 1

([A] Minor phases given in parentheses; [B] average particle diameter; [C] BET surface area; [D] void space fraction, $\Phi = 1 - \rho_{bulk}/\rho_{particle}$, where density ρ_i is in kg m^{-3}; powder bed surface ~ 33 ± 2 cm^2, bed thickness < 1 mm.)

2.2 Heating and cooling rates

The heating rates, r_H (in °C min^{-1}), of the metal nitrides in H_2 are variable, dependent on the final reaction temperature, T (in °C), and the heating time, t (in min).

For the reduction of Mn_4N and $Mn_6N_{2.58}$ with H_2, $r_H = A(T) \times t + B(T)$, where $A(T)$ is in the range of 22.1 to 41.5 °C min^{-2} (T = 300 or 550 °C) and 5.09 to 13.7 °C min^{-2} (T = 700 or 1000 °C) respectively and $B(T)$ is in the range of 108 to 126 °C min^{-1} (T = 300 or 550 °C) and 76.2 to 111 °C min^{-1} (T = 700 or 1000 °C) respectively. The Fe/Mn_4N reactant was heated in H_2 from 100 to 700°C at about 40 ± 11 °C min^{-1} and in H_2 from 100 to 750°C at about 42 ± 4 °C min^{-1}.

The heating rate during cycling $Mn_6N_{2.58}$, Ca_3N_2 and Sr_2N with H_2 between 250 and 850 °C was approximately $r_H = A \times t + B$, with A = -5.21 °C min^{-2} and B = 85.4 °C min^{-1}.

Cooling from the reaction temperature to below 100°C was rapidly at -520 to -49.5 °C min^{-1} within the first min, -88.3 to -8.81 °C min^{-1} at below 10 min, and -15.5 to -1.17 °C min^{-1} at above 10 min.

2.3 NH_3 evolution from Fe-doped Mn_4N

To assess the effect of doping with Fe on the NH_3 evolution from Mn_4N, 1.69 g of an Fe/Mn_4N mixture with about 3.8 mmol lattice nitrogen was heated consecutively in H_2 (NH_3 evolution) and N_2 (N_2 reduction). The reactant was heated in 0.5 ± 0.1 $L_{(STP)}$ H_2 min^{-1} from 100 to 700°C, held for 10 min. STP marks volumes at standard pressure and temperature, *i.e.*, 1 bar and 0°C. Liquid samples of 5 mL were taken at 0, 5 and 10 min after the reaction temperature was reached and after cooling the furnace. After XRD analysis, the solid was reintroduced into the furnace, heated from 100 to 750 °C in 0.5 ± 0.1 $L_{(STP)}$ H_2 min^{-1}, heated at 750 ± 5 °C for 10 min in 1.9 ± 0.1 $L_{(STP)}$ N_2 min^{-1}, cooled, and analyzed via XRD. The experiment was repeated in triplicate.

2.4 Effect of H_2 gas flow rate on the NH_3 yield from Ca_3N_2

The effect of the H_2 gas flow rate on the yield of NH_3 was analyzed by heating 491 ± 42 mg Ca_3N_2 (6.6 ± 0.5 mmol lattice nitrogen) for 120 min at 700°C (40 ± 2 °C min^{-1} average heating rate) in 0.19, 0.47, 0.93 and 1.86 ± 0.09 $L_{(STP)}$ H_2 min^{-1}. At 0, 1, 5, 10, 30, 60 and 120 min after reaching 700 ± 5 °C, 5 mL samples were taken from the liquid absorbent for NH_3 analysis.

2.5 Processing of experimental data

The NH_3 yield, Y_{NH3}, is reported as the molar ratio of NH_3 captured by the acidic absorbent (n in mol) at a given time, t, relative to the total lattice nitrogen of the reactant before the reaction with H_2:

$$\text{(S12)}\ Y_{NH_3} = \frac{n_{absorbedNH_3,t}}{n_N} = V_t \sum_{t=0-60\text{min}} \left(c_{NH_3,t} - c^{\#}_{NH_3}\right) \left(m_\text{r} \sum_{i=\text{all nitrides}} b_i x_i M_i^{-1} \right)^{-1}$$

where c_{NH3} in mol L^{-1} is the concentration of NH_3 detected in the absorbent, the hash symbol marks pure water used as a reference, V in L is the liquid sample volume, m_r in g is the mass of metal nitride powder reacted, b is the molar ratio of lattice nitrogen per nitride, x in g g^{-1} is the nitride weight fraction, and M in g mol^{-1} is the molar mass.

The reaction kinetics are represented best with a shrinking-core model for nitride particles with constant size limited by the chemical reaction[2]:

(S13) $k_r t = 1-(1-X_{NH_3})^{1/3}$

or by the diffusion of reaction participants through the gas film covering the particles[2]:

(S14) $k_g t = X_{NH_3}$

where k_r and k_g are specific rate constants.

3. Supporting results

3.1 Surface oxidation

Table S2: Theoretical surface reactivity

energy (eV)	reaction [A]	$Mn_2N(0001)$	$Sr_2N(0001)$
$\Delta G_{vac}[N^*,OH^*,H^*]$	$3* + N_{lat}{}^s + H_2O_{(g)} = v_N{}^s + N^* + OH^* + H^*$	-1.42	-2.71
$\Delta G_{hyd}[NH^*,OH^*]$	$v_N{}^s + N^* + OH^* + H^* = v_N{}^s + NH^* + OH^* + *$	0.19	0.54
$\Delta G_{oxi}[N^*,2H^*]$	$N_{lat}{}^s + 3* + H_2O_{(g)} = O_{lat}{}^s + N^* + 2H^*$	-0.43	-0.53
$\Delta G_{oxi,hyd}[NH^*,H^*]$	$v_N{}^s + N^* + OH^* + H^* = O_{lat}{}^s + NH^* + H^* + *$	1.13	0.08

[A]) lat and s mark the lattice nitrogen and surface; gaseous reference molecules are marked with (g); vacant surface sites and chemical species adsorbed at the surface are marked with an asterisk.

3.2 Central role of the nitrogen vacancies

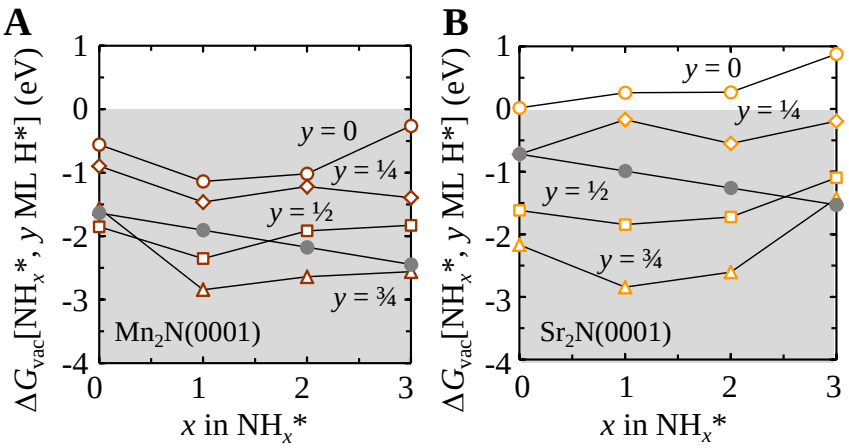

Figure S1: Free energies of forming ¼ ML v_N yielding ¼ ML NH_x^* in the presence of y = 0 (circles), ¼ (diamonds), ½ (squares), and ¾ (triangles) ML H^* on (A) $Mn_2N(0001)$ and (B) $Sr_2N(0001)$. Alternatively to the data presented in the manuscript that is assuming pre-adsorbed H^*, to compare trends, all energies are computed here assuming gas phase H_2 as the source of H^* and the hydrogen contained in NH_x^*. The total adsorption energy of x/4 ML H^* (via dissociative adsorption of H_2 from the gas phase) and ¼ ML N^* via formation of ¼ ML v_N is given for reference (gray filled circles). Lines are a guide only. The shaded regions mark exergonic surface reactions. The analysis indicates that in presence of H_2 both surfaces are expectedly covered with H^* such that NH_x^* formation at the surface may be via consumption of surface H^*. If a relative high surface coverage of ½-¾ ML H^* is to be maintained hydrogen from the gas phase may directly utilized to hydrogenate the surface nitrogen adsorbate. This is indicated by the data points that show stronger binding of the NH_x^* fragments relative to the reference shown in gray.

The free energies of the surface reactions shown with Figure 3 and Figure S1 scale mostly with the number of surface H^* adatoms and the number of hydrogen contained in the adsorbed NH_x^* species. Departures from these correlations lead partly to "crossover" of the shown trends and are due to geometric rearrangement of the adsorbates (switching of the adsorption sites) and the source of the hydrogen consumed by the reaction (surface H^* *vs*. gas phase H_2 if the H^* adatoms do not supply the entire hydrogen required for the reaction, *i.e.*, when forming ¼ ML NH_2^* in presence of ¾ ML H^* or when forming ¼ ML NH_3^* in presence of ½-¾ ML H^*). The following discusses this in more detail.

As a trend, the endergonic character of forming NH_x from lattice nitrogen of $Mn_2N(0001)$ and surface H^* becomes stronger with increasing H^* surface coverage. The deviation from this trend when forming NH_2^* or NH_3^* in presence of ¾ ML H^* *vs*. ½ ML H^* is due to a different rearrangement of the H^* adsorbates. While H^* is adsorbed at three-fold sites atop Mn in the second surface layer (TFLM), when forming N^* or NH^* in presence of ½ ML H* or ¾ ML H* (*i.e.*, in addition to the ¼ ML NH_x^*), ½ ML H^* rearranges in both cases favoring three-fold sites atop N atoms (TFLN) or atop vacancies (TFLV) in the second surface layer, respectively. That is, the rearrangement appears independent on the number of H^* adatoms and the free energy trend of the surface reactions is preserved. However, when forming NH_2^* the NH_2^* moves to a Mn-Mn bridge site (independent on the H^* surface coverage) while only at ¾ ML H^* surface coverage ¼ ML H^* changes the preferred adsorption site from TFLM to TFLV. On the other hand, when forming NH_3^* ammonia desorbs from the surface (independent on the H^* surface coverage) while the adsorption sites of the H^* adatoms at $Mn_2N(0001)$ in presence of ¼ ML v_N is preserved, relative to the adsorption sites of ½ ML H^* or ¾ ML H^* at the stoichiometric $Mn_2N(0001)$. This indicates that the departures from free energy trends when forming ¼ ML NH_2^* or ¼ ML NH_3^* in presence of ¾ ML H^* *vs*. ½ ML H^* can only partly be rationalized with adsorbate rearrangement. The fact that the formation of ¼ ML NH_3^* in presence of ½ ML H^* deviates as well from the trend, relative to the formation of ¼ ML NH_3^* in presence of ¼ ML H^* supports the conclusion that these "crossovers" are rather due to a change in the hydrogen reference energy. In all three cases ¼-½ ML hydrogen are from additional H_2 gas since the surface H^* does not supply sufficient hydrogen for the surface reactions. Still, the "crossover" of forming ¼ ML NH^* in presence of ¼ ML H^* *vs*. 0 ML H^* at $Sr_2N(0001)$ cannot be explained with gas phase H_2 as source of the hydrogen that is consumed by the reaction but correlates with different surface H^* (H^* adsorbed at different sites) consumed by forming the NH^* species.

3.3 Thermochemical reactivity of metal nitrides

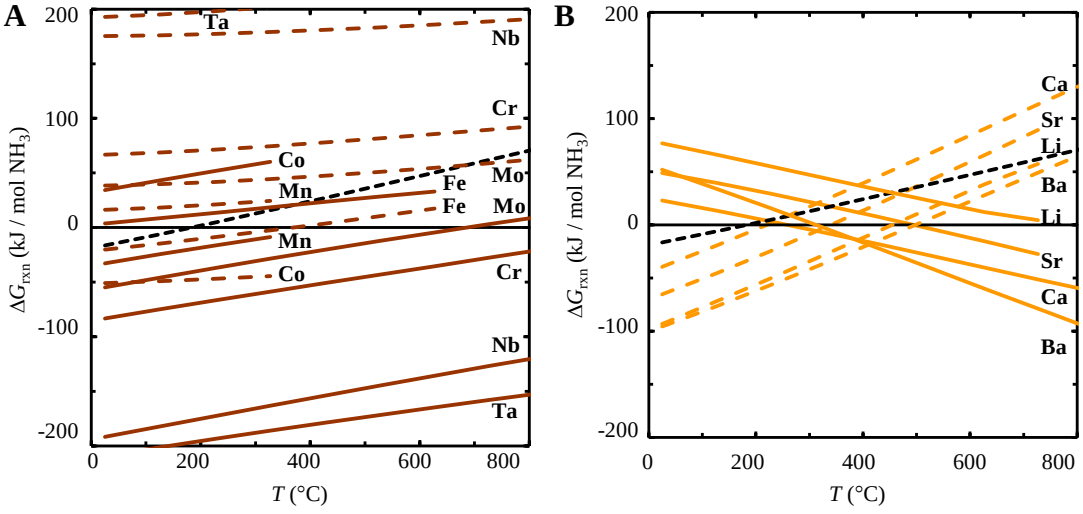

Figure S2: Ammonia synthesis at 1 bar via (A) reduction of a metal nitride with H_2 (Eq. 1, dashed lines) and N_2 reduction with the reduced metal nitrides (Eq. 2, solid lines) and (B) hydrogenation of a metal

nitride (Eq. 3, dashed line) and N_2 reduction with metal hydrides (Eq. 4, solid line). The computed materials are (A) Co_3N/Co, Fe_4N/Fe, Mn_5N_2/Mn_4N, Mo_2N/Mo, CrN/Cr_2N, TaN/Ta_2N, and NbN/Nb_2N, and (B) Li_3N/LiH, Ba_3N_2/BaH_2, Sr_3N_2/SrH_2, and Ca_3N_2/CaH_2, marked with their metallic constituents. The equilibrium of NH_3 with $3/2H_2$ and $1/2N_2$, favoring NH_3 below about 180°C, is shown as reference at 1 bar (dotted line). While the N_2 reduction with metal hydrides may form NH_3 (*i.e.*, the superposition of ΔG_{rxn} of the N_2 reduction and the NH_3 equilibrium with N_2/H_2) at low temperatures, which is expected to increase the yield of the metal nitride slightly, this will not change the endergonic character of the shown reaction equilibria at the computed temperatures.

The correlation of the thermochemical equilibrium of the NH_3 evolution at 25°C with N_dE_d was computed for the Co_3N/Co, Fe_4N/Fe, Mn_5N_2/Mn_4N, Mo_2N/Mo, CrN/Cr_2N, TaN/Ta_2N, and NbN/Nb_2N pairs; the analogous correlation with N_sE_s was computed for the Li_3N/LiH, Ba_3N_2/BaH_2, Sr_3N_2/SrH_2, and Ca_3N_2/CaH_2 pairs. The number of electrons and the energy of these electrons in a given ground state are taken from the electronic structure code DACAPO.[3] We note the trend of the reaction energetics of the alkaline earth metal nitrides with the bonding valance s-electrons in the metal ground state does not apply to Be and Mg constituents which do not form thermally stable metal hydrides at ambient pressure.[4]

3.4 NH_3 evolution from Fe-doped Mn_4N

One possibility to control the reactivity of the lattice nitrogen at the surface is to weaken the strength of the chemical bond formed between manganese and nitrogen. This may be achieved via doping the metal nitride with a metal,[5,6] such as iron, that forms only weak metal-nitrogen bonds. Figure S3 shows the ammonia yield from Fe-doped Mn_4N, equimolar in Fe/Mn. The sample was cycled three times; after 10 min in H_2 at 700°C, 3.3, 2.1, and 2.0 mol% NH_3 were formed in the cycles. This shows no significant improvement compared to 2.7 mol% after 10 min at 700°C in the absence of Fe, which is shown with Figure 6. In agreement with the relatively slow reaction kinetics of manganese nitride discussed above, Figure S3 shows that the concentration of the lattice nitrogen throughout the NH_3 evolution and N_2 reduction remained constant within the analytical uncertainty. We note, a full assessment of the effect of iron on the strength of the manganese-nitrogen bond requires testing of a ternary metal nitride or nanocomposite. However, the present results suggest that iron diminishes the yield of the ammonia evolution, which can be understood due to the catalytic activity of iron in establishing the chemical equilibrium in NH_3, N_2 and H_2 gas mixtures.[7]

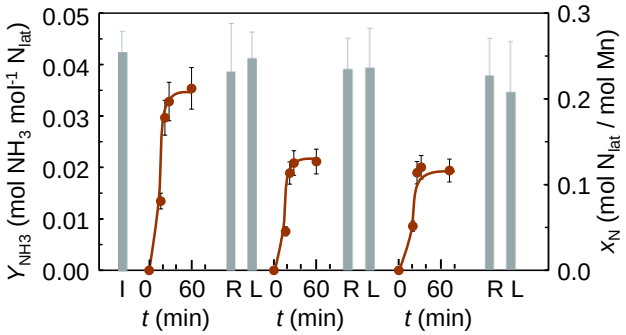

Figure S3: Ammonia yield (red circles, lines to guide the eye ± 11.43% via error propagation) from Fe-doped Mn_4N heated successively in H_2 at 700°C and 1 bar (data points are before heating, when reaching 700°C, 5 or 10 min after reaching 700°C, after cooling). The molar ratio of the lattice nitrogen (bars, ± 26.75% via error propagation) was analyzed (I) initially, (R) after the reaction with H_2, and (L) after subsequent heating for 10 min in N_2 at 750°C and 1 bar.

3.5 Ammonia via metal nitride hydrogenation

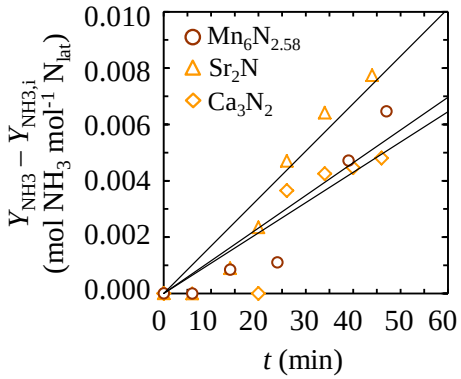

Figure S4: To estimate the NH_3 formation rates from the reaction of metal nitrides with H_2, the difference between the NH_3 yield at a given time point, Y_{NH3}, and the initial NH_3 yield, $Y_{NH3,i}$, from the reaction of $Mn_6N_{2.58}$, Ca_3N_2, and Sr_2N with H_2 at 1 bar and 220-850°C. Solid lines are linear fits.

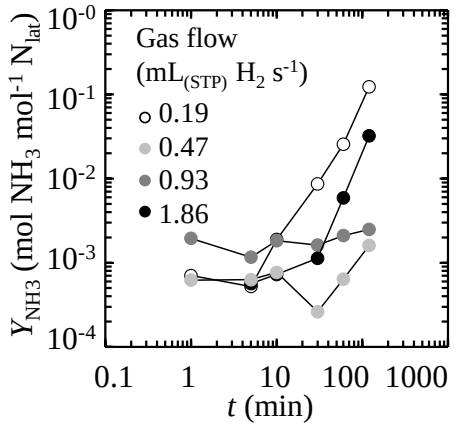

Figure S5: NH_3 yield from the reaction of Ca_3N_2 with various flow rates of H_2 (given at standard temperature and pressure, STP, *i.e.*, 1 bar and 0°C) at 1 bar and 700°C *vs*. time. Error propagation of the NH_3 yield within a 95% confidence interval (error bars omitted for clarity) yields in average about ± 26.58%. Solid lines are a guide only.

4. References

(1) ASE is open-source code available from the Department of Physics at the Technical University of Denmark and available at https://wiki.fysik.dtu.dk/ase/.

(2) Levenspiel, O. *Chemical reaction engineering, Third Edition, Chapter 25 Fluid-particle reactions: Kinetics*; John Wiley & Sons: New York, **1999**.

(3) https://wiki.fysik.dtu.dk/dacapo/Pseudopotential_Library.

(4) Barin, I. *Thermochemical Data of Pure Substances;* VCH Verlagsgesellschaft mbH, 0-6940 Weinheim, Federal Republic of Germany, **1993**.

(5) Hunter, S. M.; McKay, D.; Smith, R. J.; Hargreaves, J. S. J.; Gregory, D. H. *Chemistry of Materials* **2010**, *22*, 2898-2907.

(6) Jacobsen, C. J. H.; Dahl, S.; Clausen, B. S.; Bahn, S.; Logadottir, A.; Nørskov, J. K. *Journal of the American Chemical Society* **2001**, *123*, 8404-8405.

(7) Ertl, G. *Angewandte Chemie-International Edition* **2008**, *47*, 3524-3535.